Journal of Ceramic Processing Research. Vol. 25, No. 6, pp. 1115~1121 (2024)
(Received 9 August 2024, Received in revised form 7 November 2024, Accepted 18 December 2024)
https://doi.org/10.36410/jcpr.2024.25.6.1115

J O U R N A L O F
Ceramic Processing Research

Synthesis of nano-scale silicon powder by magnesiothermic reduction for anodes in lithium-ion battery

Ju-Chan Kwon[a] and Sang-Jin Lee[a,b,*]
[a]*Department of Advanced Materials Science and Engineering, Mokpo National University, Muan 58554, Republic of Korea*
[b]*Research Institute of Ceramic Industry and Technology, Mokpo National University, Muan 58554, Republic of Korea*

Pure Si powder used as an anode material can enhance the capacity of lithium ion batteries. However, repeated charging and discharging can cause significant volume expansion, thereby reducing the durability and battery life cycles. Using round-shape, nanoscale Si powder, which can be fabricated by a reduction process of spherical SiO_2 powder, can relieve this problem. This reduction method results in the formation of SiO_x including Si structure. In particular, approaches such as using nano powder as a starting material or employing a high-energy milling process to produce nano powder have been extensively explored in recent research. In the present study, nano-sized SiO_x powder containing Si was fabricated by using 100 nm synthetic, spherical SiO_2 powder and commercial Si powder as the starting material. The materials were mixed by a high-energy milling process using an attrition mill and then subjected to magnesiothermic reduction heat treatment. In particular, NaCl was used during the heat treatment to inhibit the formation of Mg_2SiO_4 reactant. The crystallinity and the Si-O-Si bonding state of the final SiO_x powder, obtained after acid treatment and DI water washing, were examined by characterization using X-ray diffraction, Fourier transform infrared spectroscopy, and X-ray photoelectron spectroscopy.

Keywords: Spherical silica, Nano silicon, Attrition milling, Magnesiothermic reduction, SiO_x powder.

Introduction

Increasing the capacity of Li-ion batteries has recently become a significant issue owing to their growing use in mobile phones and hybrid and battery electric vehicles (EVs) [1]. Graphite is commonly used as the anode, where each carbon atom is bonded to two other carbon atoms in a regular hexagonal pattern, thereby forming thin layer plates [2]. This layered structure facilitates the Li ion transport, thus making graphite a suitable anode material. With the sharp increase in the demand for EV batteries, the use of Si as an anode is also gaining momentum. In particular, Si anodes increase the capacity of the battery by tenfold per gram, thereby extending the driving range of EVs. However, Si and graphite absorb Li by different mechanisms, and this results in significant volume expansion in the case of Si [3-5]. Specifically, Si anodes undergo a significant volume expansion owing to repeated charging and discharging, resulting in reduced durability of the active material and life cycle of the battery.

This limitation of Si anodes can be addressed by mixing a specific quantity of nano Si with graphite to minimize volume expansion. However, the high cost of nano Si remains a crucial problem. Researchers recently have focused on preventing the volume expansion of Si by synthesizing nano-sized SiO_x. Kong et al., coated Si particles with SiO_x by using an oxidation process; the SiO_x coating thickness was 3.4~9.6 nm, which helped alleviate the sudden volume expansion of Si and facilitated the dispersion of Li ions [6]. Chen et al., investigated the production of SiO_x, which is primarily composed of Si, through magnesiothermic reduction using SiO_2 as the starting material [7]. They observed that the loose structure of multiporous Si could effectively manage volume changes during the charging and discharging processes. Cho et al. [8] investigated the cost reduction in Si fabrication through magnesio-milling of SiO_2-Mg mixed powder using a planetary mill and attrition mill equipment.

In this study, the fabrication of Si nano-sized powder containing $SiO_{(0<X<2)}$ was examined. Spherical amorphous SiO_2 powder prepared via the Stöber synthesis process [9] and commercial Si powder were used as the starting material. The starting powder was subjected to nanoscale pulverizing mixing through planetary milling, which is a high-energy milling process, to facilitate the reduction process. Subsequently, nano Si was fabricated via a magnesiothermic reduction process with the addition of NaCl to inhibit the formation of by-products. The by-products were removed by acid treatment and washing with water. Fourier transform infrared spectrometry (FT-IR) and X-ray photoelectron spectroscopy (XPS) were

*Corresponding author:
Tel : +82-61-450-2493
Fax: +82-61-450-2498
E-mail: lee@mnu.ac.kr

employed to analyze the bonding state between Si and oxygen in the synthesized SiO_x powder including nano Si.

Experimental Procedure

Fabrication of nano SiO_x anode material

A 100 nm amorphous, spherical SiO_2 powder synthesized by the Stöber process, and commercial Si powder (99.99%, 10~80 μm, Samchun Chemicals, Korea) were used as the starting material. A sealed planetary mill container (water-cooled, Nano Ceratech, Korea), with, 1,000 zirconia balls having a radius of 3 mm and 500 zirconia balls having a radius of 5 mm was employed to ensure uniform mixing. The synthesized SiO_2 and Si powders were added into the container at a mass ratio of 1:1. Subsequently, pulverizing and mixing were conducted by ball milling at 400 rpm for 24 h [10].

Before adding Mg to the planetary milled powder, NaCl powder was mixed (planetary milled powder : NaCl (in wt%) = 1:0.8) to inhibit excessive production of MgO and its by-products. The mixed powder with deionized (DI) water was stirred at 50 °C for 3 h and then vacuum-dried at 80 °C for 24 h. The agglomerated dried powder was pulverized in an alumina mortar. Subsequently, Mg powder (98.5%, 100~150 μm, Daejung Chemicals & Metals, Korea) was added at a SiO_2 starting powder : Mg weight ratio of 1:1 and dry mixed at 100 rpm for 5 h using a dry powder mixer. For comparison another reduction material, $Mg(NO_3)_2$ was also assessed. It was wet-mixed at a SiO_2 starting powder : Mg weight ratio of 1:1, and then dried. The final mixed powders underwent a magnesiothermic reduction process. For the heat treatment process, the temperature was increased to 800 °C at a rate of 5 °C/min in a vacuum atmosphere using a vacuum furnace (electric & vacuum furnace, Pyro Tech, Korea), and held for 3 h. The heat-treated sample was rinsed multiple times with DI water to remove NaCl and subsequently submerged in a 2 M hydrochloric acid solution for 24 h to convert the residual Mg by-products into a highly soluble substance. Furthermore, any remaining SiO_2 was eliminated by soaking the sample in a 5% hydrofluoric acid (HF) solution for 1 h. The sample was then washed with ethanol and dried at 105 °C for 4 h to eliminate surface moisture, after rinsing several times with DI water.

Characterization

An X-ray diffraction (XRD) analyzer (X'pert-pro MPD, PANalytical, Netherlands) was employed to examine the variations in the crystalline structure after each process. The particle size of the starting Si powder and SiO_2 and Si powder mixtures after planetary milling was measured

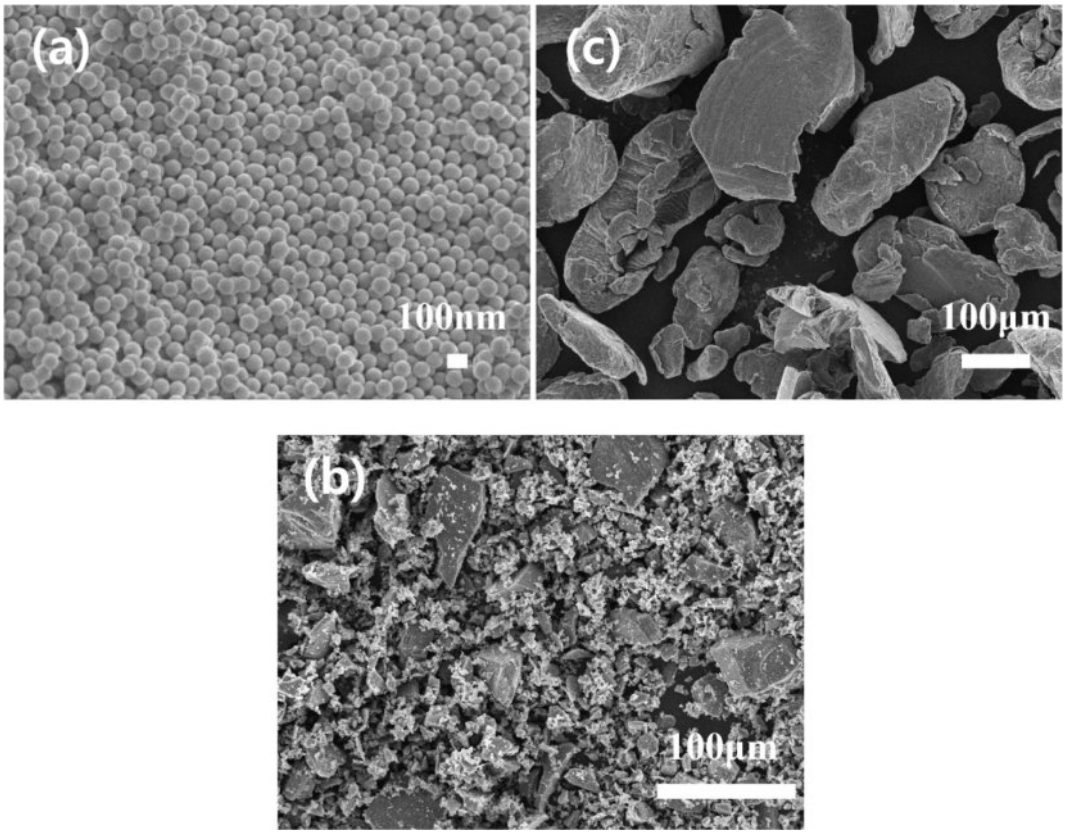

Fig. 1. FE-SEM micrographs of (a) spherical SiO_2 powder prepared via Stöber process, (b) commercial Si powder, and (c) commercial Mg powder.

by laser diffraction analysis (LS13 320, Beckman Coulter, USA). The ultrasonic dispersion of the powder slurry was carried out for 15 min. The microstructure of the powders for each experiment condition was examined using field-emission scanning electron microscopy (FE-SEM, JSM-7100F, Jeol, Japan). The sample was affixed to an Al holder using carbon tape and coated with Au-Pd sputtering. To analyze the atomic bonding structure of the powders at each processing stage, Fourier transform infrared spectroscopy (FT-IR, Vertex 80v, Bruker, USA) was performed within the range of 3,500~500 cm^{-1}. Finally, X-ray photoelectron spectroscopy (XPS, PHI Quantera II, ULVAC-PHI, Japan) was employed to examine the atomic structure of the surface composition of the sample with an Al-K_α (1,186 eV) source under a chamber pressure of 2×10^{-7} Pa.

Results and Discussion

The microstructures of the synthesized SiO_2 powder, commercial Si powder, and Mg powder are shown in Fig. 1. The synthesized SiO_2 powder exhibits uniformly 100 nm sized spherical shapes, whereas the Si powder displays a broad particle-size distribution. The Si powder was pulverized using high-energy planetary milling, and reacted with O_2 in the SiO_2 powder [11, 12]. Micro-sized particles were excluded from the Mg powder used as a reducing agent to minimize the formation of by-products resulting from reactions with the planetary ball milled SiO_x. Fig. 2 represents the particle size distribution of the Si powder before and after high-energy planetary milling. The starting Si powder exhibited a broad particle size distribution. After planetary milling, the decreasing trend was dramatical showing the size distribution of below 1 μm to nano size.

The XRD results of the mixed Si and SiO_2 powders before and after planetary milling are presented in Fig. 3. A distinct crystalline Si peak is observed before milling owing to the influence of the metallic Si powder, whereas the amorphous SiO_2 peak from the synthesized SiO_2 powder is less pronounced. After planetary milling, the crystalline Si peak is not clearly visible, and only the amorphous SiO_2 peak is observed at approximately 25° (Fig. 3(a)). The magnified image (Fig. 3(b)) reveals an amorphous phase with a small Si peak, which is likely due to the pulverization of large Si particles into nanoscale sizes through high-energy milling. During this process, Si extensively reacts with O_2 in SiO_2, forming SiO_x (Si, if x = 0).

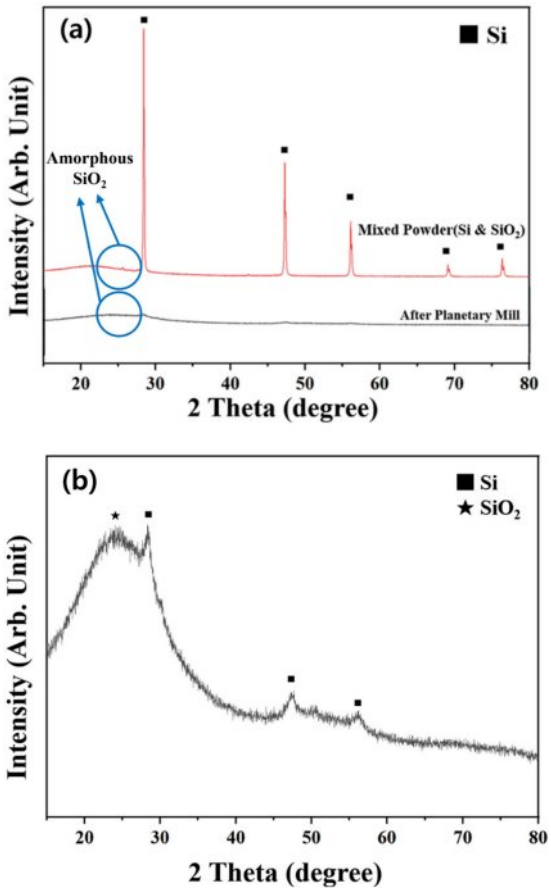

Fig. 3. (a) XRD patterns of mixed Si and SiO_2 powders before and after planetary milling and (b) corresponding magnified pattern after planetary milling.

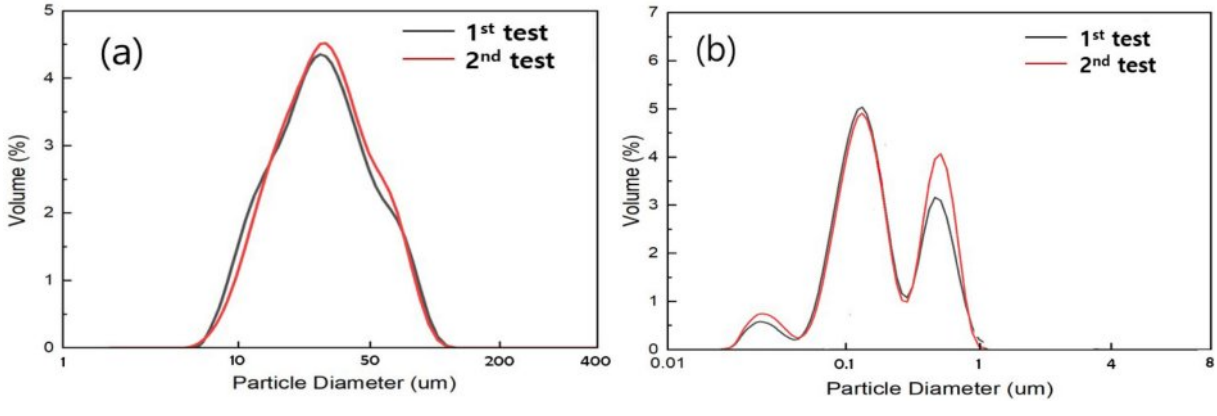

Fig. 2. Particle size distribution of (a) commercial Si powder and (b) SiO_2 and Si powder mixtures after planetary milling.

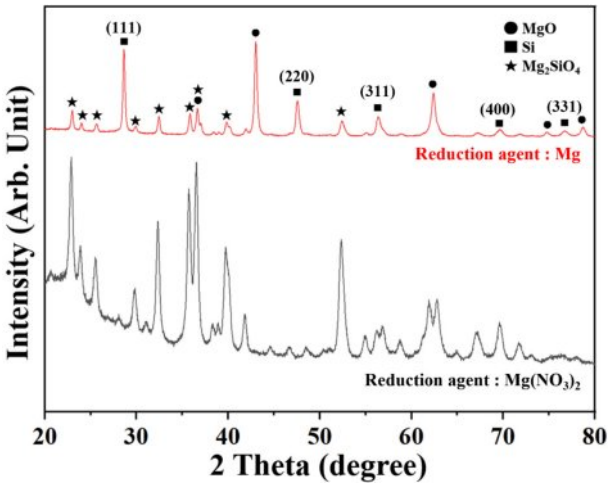

Fig. 4. XRD patterns of magnesiothermic reduction of SiO_x powder according to reducing agent without NaCl addition.

The changes in the crystalline structure of the SiO_x powder after the addition of Mg or $Mg(NO_3)_2$ as a reducing agent and the vacuum heat treatment are shown in Fig. 4. In both cases, the samples were fabricated without adding NaCl. When the Mg powder was used as the reducing agent, oxidized MgO, reactant Mg_2SiO_4, and crystalline Si peaks were observed. As an amorphous SiO_2 peak was not observed at approximately 25°, most of the amorphous SiO_x powder is considered to be reduced through the reduction process or formed a reactant with Mg. Chen et al., synthesized mesoporous Si through magnesiothermic reduction by performing heat treatment at 650 °C in a N_2 atmosphere. An the XRD analysis of the synthesized particles revealed Si (111), (220), (311), (400), and (331) peaks, whereas MgO, Mg_2Si, and Mg_2SiO_4 were observed as by-products [7, 13-15]. In this experiment, heat treatment was conducted at 800 °C in a vacuum atmosphere. Si synthesized through reduction displayed clear peaks on five crystalline planes, consistent with the findings of Chen et al. [7]. However, Mg_2Si was not observed, suggesting that the reduced Si did not react with Mg in the vacuum atmosphere. In the previous study, for the reduction of spherical monodisperse silica particles, a nitrogen gas atmosphere mixed with 5% hydrogen was applied without Mg powder, and carbothermal reduction method was also tried by adding some carbons to selectively remove oxygen atoms in the silica. However, crystalline Si peak was not observed in the XRD examination [16, 17].

$Mg(NO_3)_2$ was wet-mixed and used as a reducing agent to improve the blend homogeneity with the SiO_x powder; In this study, a reducing effect was not achieved. In addition to amorphous SiO_x peaks at around 2θ 25°, peaks of Mg_2SiO_4 were observed. The Mg ions had already reacted with O_2 during the drying process, resulting in amorphous MgO, and then reacted with SiO_x during heat treatment, thereby generating Mg_2SiO_4.

Fig. 5 reveals the microstructure of the powder, which underwent magnesiothermic reduction with Mg as the reducing agent. Fig. 5(a) shows reduced SiO_x powder and the MgO or Mg_2SiO_4 by-products. Large sized by-products (red circles) were formed when the smaller Mg particles reacted with amorphous SiO_x during heat treatment. The magnified image of the nano-sized spherical particles shown in Fig. 5(b) depicts the reduced spherical SiO_2 starting powder. The partially fractured and agglomerated particles originate from the SiO_x and commercial Si powder obtained through planetary milling with pulverization.

The formation of a by-product of Mg_2SiO_4 was inhibited by the addition of NaCl during heat treatment, and after heating the NaCl was removed by rinsing with DI water. The XRD and FE-SEM results of the finally obtained powder are represented in Fig. 6. The XRD spectra do not include peaks of Mg, MgO, and Mg_2SiO_4, and only crystalline Si and amorphous SiO_x peaks are observed. The added NaCl inhibits the reaction between SiO_x and MgO by absorbing the surrounding heat during melting, which has a high enthalpy level, in a reducing atmosphere [18-20]. Mg is therefore present as MgO rather than as a Mg_2SiO_4 reactant. Mg and MgO are converted into highly soluble MgCl

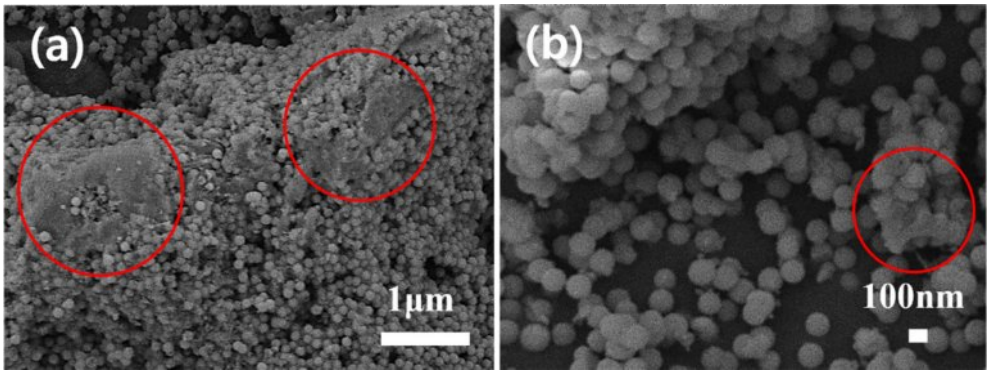

Fig. 5. FE-SEM micrographs of (a) magnesiothermic reduction of SiO_x powder using Mg as the reducing agent without the addition of NaCl and (b) magnified image of SiO_x powder in (a).

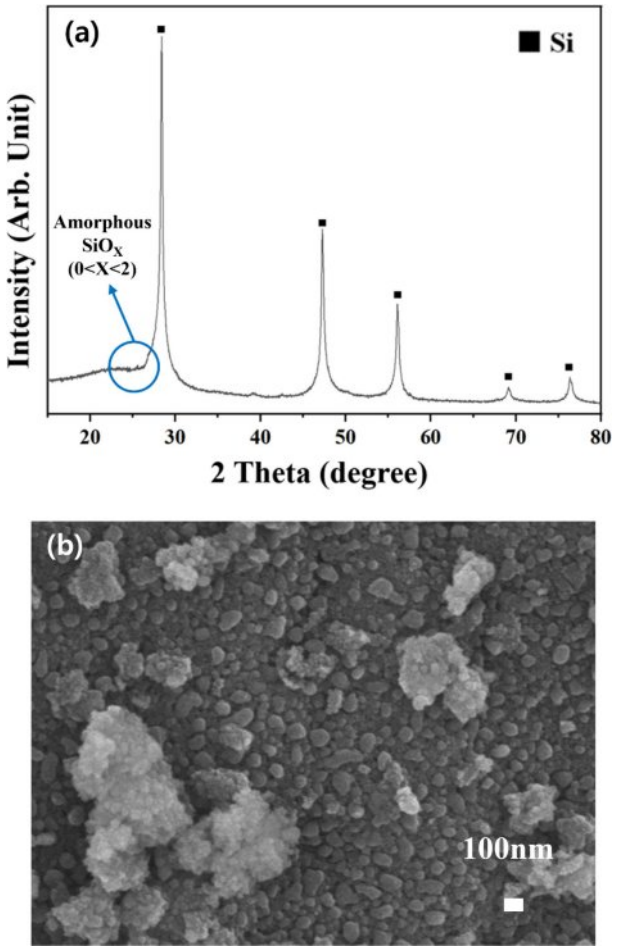

Fig. 6. (a) XRD patterns of magnesiothermic reduction of SiO_x powder with addition of NaCl, water washing, and acid treatment. (b) FE-SEM micrograph of Si powder from (a).

through HCl treatment and removed after rinsing with water [15]. Furthermore, the residual amorphous SiO_x is dissolved through HF acid treatment and eliminated to a certain extent. Amorphous SiO_x peaks are still observed at approximately 25°, indicating that the starting SiO_2 powder is not entirely reduced to Si (where $_X = 0$ in SiO_x) and partially remains in an amorphous SiO_x state [21]. The microstructure analysis revealed the agglomeration of some pulverized powder owing to the planetary milling, drying, and heat treatment processes. The complete spherical form was lost during acid treatment, resulting in particle sizes of approximately 100 nm. The agglomerated powders during the several processes are due to the fine particles of nano size, and the powders seem not to have an influence on the capacity of silicon anode [22].

A FT-IR analysis was conducted on the Si and SiO_2 powders used as starting materials, powders after planetary milling, and the final powder after magnesiothermic reduction and acid treatment. The changes in the Si–O–Si bonding of each sample are displayed in Fig. 7. The variations in the intensity of the Si–O–Si bonding are

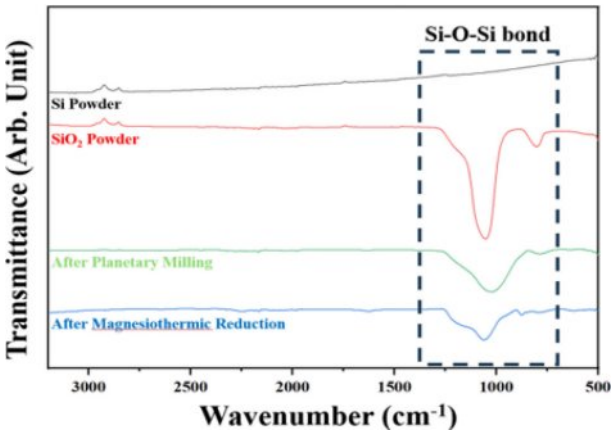

Fig. 7. FT-IR spectra of starting Si and amorphous SiO_2 powders, planetary-ball-milled powder, and final reduced powder obtained by applying the magnesiothermic reduction process after acid treatment and rinsing with DI water.

notable around the wavenumber of 1,000 cm^{-1} [23, 24]. The FT-IR spectra of Si powder (the starting material) do not display any Si–O–Si bonding peaks. In contrast, the synthesized SiO_2 powder, which consists of a SiO_4 tetrahedron structure, exhibits the most prominent peaks. Subsequently, the intensity of the peaks corresponding to Si–O–Si bonding decreases after planetary ball milling and magnesiothermic reduction. Specifically, the peaks of Si–O–Si bonding in the spectra of the final powders, which underwent magnesiothermic reduction and acid treatment, suggest the formation of an oxide film on the surface of the Si powder due to oxidation when exposed to air during the sample preparation process involving the residual amorphous SiO_x ($x > 0$) powder.

An XPS analysis was performed based on the FT-IR spectroscopy results to further evaluate the Si–O–Si bonding state at approximately 1,000 cm^{-1}, and the results are shown in Fig. 8. As the Si2p peak is detected for all sample powders, the x value of SiO_x can be analyzed by examining the narrow range of this peak [25, 26]. In the study conducted by Miyachi et al. [27] a XPS analysis revealed that SiO_x can be characterized as Si^{0+}(Si) when $x = 0$ or Si^{4+}(SiO_2) when $x = 2$. The x value continuously varies within the binding energy range of 98-104 eV. With decreasing binding energy, the SiO_x state with a low oxygen content becomes more apparent. In the narrow range graph corresponding to Si2p (Fig. 8(b)), peaks of the Si powder are observed with binding energy of approximately 98.5 and 102.5 eV. Each peak corresponds to Si^{0+} and Si^{3+}, representing Si and SiO_x ($1.5<x<2.0$). The presence of the peak at 102.5 eV corresponding to Si^{3+} in the spectra of the Si powder is attributed to the formation of an oxide layer resulting from the oxidization of the particle surface of the Si powder exposed to O_2 in air. Meanwhile, the peak of the SiO_2 powder is observed at the binding energy of 104 eV, with $x = 2$, indicating a SiO_2 state corresponding to stable Si^{4+}. The peak corresponding to Si^{4+} shifts to

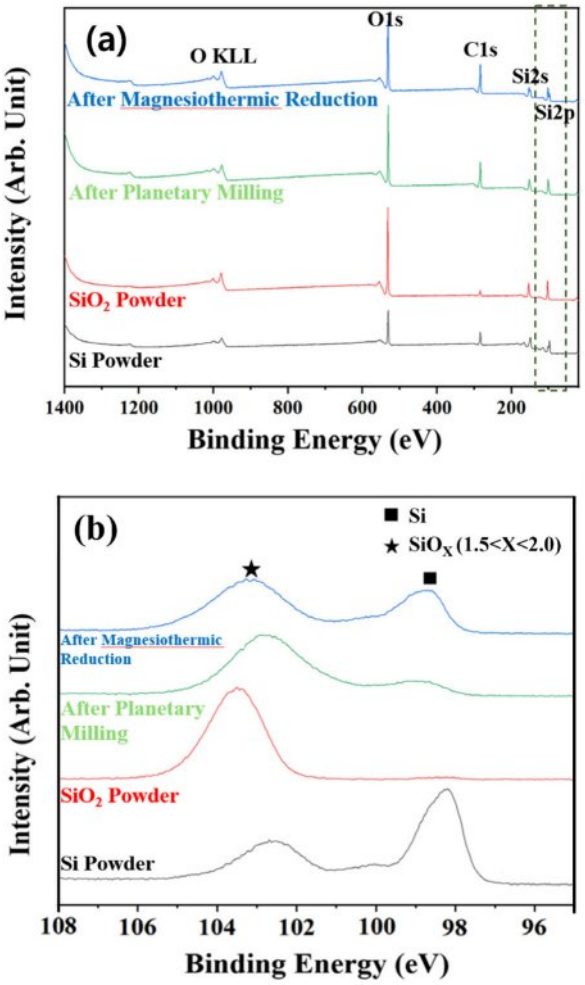

Fig. 8. (a) XPS result of the starting Si and amorphous SiO_2 powder, planetary-ball-milled powder, and final reduced powder obtained by applying the magnesiothermic reduction process and acid treatment. (b) Narrow range spectra of the Si2p peak.

the right after planetary milling and magnesiothermic reduction. After planetary milling, the peak further shifts to the right of 104 eV, indicating a SiO_x state with less oxygen than SiO_2. Additionally, the peak at 98.5 eV suggests the presence of Si. After magnesiothermic reduction, the peak at 98.5 eV becomes more prominent. This indicates the presence of Si powder in the SiO_x ($x<2$) state detected from residual SiO_x including oxygen and oxide film on the surface. The oxide film in the SiO_x will help to alleviate the sudden volume expansion or lessen the capacity [22]. A further study with more focus on the electrochemical properties will be done to investigate the effect of the oxide film of SiO_x.

Conclusions

Spherical and amorphous SiO_2 powder having a particle diameter of 100 nm was synthesized by the Stöber process and then reduced to produce nano scale SiO_x powder containing Si, which is suitable for use as anode materials in lithium ion batteries. Commercial Si powder was added to the synthesized SiO_2 powder, and SiO_x powder was prepared via planetary milling. Subsequently, Mg powder was added, and the mixture underwent heat treatment in a vacuum. The thermally reduced powder was then subjected to acid treatment and DI water washing to remove the residual Mg by-products. The XRD analysis of the finally fabricated SiO_x powder revealed a mixture of metallic Si and amorphous SiO_x. FT-IR spectroscopy and XPS analyses of the fabricated SiO_x powder were conducted to determine the x value, which varied in the range of 0~2, thereby confirming the presence of Si as Si^{0+} and amorphous type SiO_x ($0<x<2.0$). In the magnesiothermic reduction process, NaCl was included to prevent the formation of Mg_2SiO_4, and the highly soluble MgCl realized through HCl treatment was removed after rinsing several times with DI water.

Acknowledgements

This work was supported by Research Funds of Sabbatical Year of Mokpo National University in 2024.

References

1. M. Gu, Y. He, J. Zheng, and C. Wang, Nano Energy 17 (2015) 366-383.
2. H. Zhang, Y. Yang, D. Ren, L. Wang, and X. He, Energy Storage Mater. 36 (2021) 147-170.
3. J. Guo, X. Chen, and C. Wang, J. Mater. Chem. 20 (2010) 5035-5040.
4. B. Jarulertwathana and T. SaraKonsri, J. Ceram. Process. Res. 15[6] (2014) 389-392.
5. J. Lee, Y Ahn, and S. Lee, J. Ceram. Process. Res. 24[6] (2023) 1010-1024.
6. K. Kong, G. Xu, Y. Lan, C. Jin, Z. Yue, X. Li, F. Sun, H. Huang, J. Yuan, and L. Zhou, Appl. Surf. Sci. 515 (2020) 146026.
7. W. Chen, Z. Fan, A. Dhanabalan, C. Chen, and C. Wang, J. Electrochem. Soc. 158[9] (2011) A1055-A1059.
8. W.C. Cho, H.J. Kim, H.I. Lee, M.W. Seo, H.W. Ra, S.J. Yoon, T.Y. Mun, Y.K. Kim, J.H. Kim, B.H. Kim, J.W. Kook, C.Y. Yoo, J.G. Lee, and J.W. Choi, Nano Lett. 16 (2016) 7261-7269.
9. J.C. Kwon, B.H. Oh, and S.J. Lee, Korean J. Mater. Res. 33[12] (2023) 530-536.
10. Y.T. Park and K.T. Lee, J. Ceram. Process. Res. 17[1] (2016) 1-4.
11. B.E. Nilssen and R.A. Kleiv, SN. 12[10] (2020) 2413-2423.
12. T.T.T. Hien, T. Shirai, and M. Fuji, J. Ceram. Soc. Jpn. 120[10] (2012) 429-435.
13. I.S. Curtis, R.J. Wills, and M. Dasog, Nanoscale 13 (2021) 2685-2692.
14. A. Rasouli, M. Tsoutsouva, J. Safarian, and G. Tranell, Materials 15[19] (2022) 1-14.
15. Y. Iwadate, K. Ohgane, and T. Ohkubo, Electrochemistry (Tokyo, Jpn.) 86[4] (2018) 198-201.
16. P. Lv, H. Zhao, C. Gao, T. Zhang, and X. Liu, Electrochim. Acta, 152 (2015) 345-351.

17. J. Yang, T. Mori, and M. Kuwabara, ISIJ Int. 47[10] (2007) 1394-1400
18. J. Entwistle, A. Rennie, and S. Patwardhan, J. Mater. Chem. A. 6[38] (2018) 18344-18356.
19. C. Li, C. Liu, W. Wang, Z. Mutlu, J. Bell, K. Ahmed, R. Ye, M. Ozkan, and C.S. Ozkan, Sci. Rep. 7[917] (2017) 1-11.
20. Z. Favors, W. Wang, H.H. Bay, Z. Mutlu, K. Ahmed, C. Liu, M. Ozkan, and C.S. Ozkan, Sci. Rep. 4 (2014) 1-7.
21. J. Yang, Y. Takeda, N. Imanishi, C. Capiglia, J.Y. Xie, and O. Yamamoto, Solid State Ionics. 152-153 (2002) 125-129.
22. J.K. Lee and J.R. Yoon, J. Ceram. Process. Res. 21[5] (2020) 533-538.
23. G. Kandilioti, A. Siokou, V. Papaefthimiou, S. Kennou, and V. G. Gregoriou, Appl. Spectrosc. 57[6] (2003) 628-635.
24. Y. Park, M. Boyer, G.S. Hwang, and J. Lee, J. Electroanal. Chem. 833 (2019) 552-559.
25. W. Wu, M. Wang, R. Wang, D. Xu, H. Zeng, C. Wang, Y. Cao, and Y. Deng, J. Power Sources. 407 (2018) 112-122.
26. Y. Park, Y. Myung, and J. Lee, ACS Appl. Energy Mater. 3 (2020) 8803-8811.
27. M. Miyachi, H. Yamamoto, H. Kawai, T. Ohta, and M. Shirakata, J. Electrochem. Soc. 152[10] (2005) A2089-A2091.